Discover Oncology

RESEARCH Open Access

Comprehensive multi-omics analysis of histone acetylation modulators identifies ASH1L as a novel aggressive marker for osteosarcoma

Chenlie Ni[1†], Qiwen Sun[2†] and Haibo Yin[1*]

†Chenlie Ni and Qiwen Sun have made equal contributions to this work.

*Correspondence:
Haibo Yin
HaiboY88899@163.com
[1]The Second Affiliated Hospital of Jiaxing University, Jiaxing 314000, China
[2]Haining Yuanhua Township Central Health Hospital, Jiaxing 314000, China

Abstract

Background Osteosarcoma, a highly malignant bone tumor prevalent in children and adolescents, continues to have poor long-term survival rates, particularly in metastatic cases. While histone acetylation dysregulation has been implicated in cancer progression, the role of histone acetylation modification-related proteins (HAMRPs) in osteosarcoma immune infiltration and prognosis remains unclear.

Methods The expression patterns, prognostic implications, and clinical correlations of HAMRPs in osteosarcoma were analyzed using the TARGET, GEO, TISCH, and HPA databases. The effectiveness of HAMRPs in predicting the immune landscape of osteosarcoma was confirmed using CIBERSORT, ssGSEA, and ESTIMATE algorithms. The study employed GSEA analysis, wound healing assay, Transwell, and western blot to explore the role and regulatory mechanism of the key gene ASH1L in osteosarcoma progression.

Results Two distinct histone acetylation modification patterns were identified, showing significant differences in survival, clinical features, and immune landscape. Comprehensive clinical correlation analysis and Kaplan-Meier analysis of all HAMRPs used for two subtypes revealed that higher ASH1L expression was found in metastatic osteosarcoma cases and indicated poorer survival outcomes. In vitro experiments confirmed that ASH1L promoted osteosarcoma metastasis and epithelial-mesenchymal transition via the AKT/mTOR pathway. Additionally, an ASH1L-derived risk model was developed to aid personalized clinical decisions.

Conclusions This study elucidates the prognostic and immunological significance of HAMRPs and highlights ASH1L as a novel aggressive marker in osteosarcoma.

Keywords Osteosarcoma, Multiomics analysis, Histone acetylation modulators, ASH1L, Aggressive marker

1 Introduction

Osteosarcoma, a highly aggressive bone malignancy with molecular heterogeneity, remains a leading cause of cancer mortality in children and adolescents [1–3]. The global burden of osteosarcoma continues to escalate, driven by its propensity for recurrence,

metastatic dissemination, and dismal long-term outcomes [4–7]. While current treatment combines surgery with neoadjuvant/adjuvant chemotherapy [8–10], options remain limited for metastatic or recurrent cases. The disease shows striking pulmonary tropism, with lung metastases causing most fatalities [11]. Before effective chemotherapy, 85% of localized cases developed lung metastases post-local treatment [12]. Currently, metastatic osteosarcoma maintains a dismal 15–30% 5-year survival rate, with no major therapeutic breakthroughs in decades [13, 14], highlighting the critical need for predictive biomarkers and precision therapies.

Chromatin architecture, nucleosome stability, and transcriptional regulation are primarily orchestrated by histones [15–18]. As highly conserved nuclear proteins in eukaryotes, histones possess a strong positive charge and assemble into histone octamers, forming the structural core of nucleosomes [19]. These canonical histones play a pivotal role in genome compaction by wrapping DNA into nucleosomal units, thereby facilitating critical cellular processes such as transcription, replication, and DNA repair [20].

Cancer genomics reveals frequent mutations in epigenetic regulators [21]. Among these, histone modifications constitute a fundamental layer of epigenetic regulation, profoundly shaping gene expression and the interpretation of genetic information [22, 23]. Histones undergo a diverse array of post-translational modifications (PTMs), which serve as dynamic epigenetic marks and modulate their interactions with DNA [24]. To date, numerous PTMs have been identified, including methylation, acetylation, propionylation, butyrylation, lactylation, ubiquitination, phosphorylation, and citrullination, among others [25–28]. These modifications frequently occur in combinatorial patterns, collectively forming the "histone code"—a sophisticated regulatory mechanism that vastly expands the informational potential of the genetic code [16, 29]. The histone code exerts widespread influence over diverse biological processes, including cell metabolism, differentiation, senescence, chromatin remodeling, DNA repair, and transcriptional regulation [28]. The functional consequences of these modifications depend on multiple factors, such as PTM type, histone variant, and the precise amino acid residue targeted [30].

Histone acetylation, one of the earliest discovered histone PTMs, exists as both internal lysine and N-terminal modifications [31, 32]. This modification typically induces chromatin relaxation, facilitating transcriptional machinery recruitment and enhancing gene expression [33]. The dynamic equilibrium between histone acetyltransferases (HATs) and histone deacetylases (HDACs) tightly regulates this process, playing pivotal roles in chromatin remodeling and transcriptional control [34–37]. HDACs restore lysine positive charges by removing acetyl groups, thereby suppressing gene transcription [38]. In osteosarcoma, HDAC1/2 inhibition has demonstrated anti-metastatic effects [39], with mechanistic studies showing HDAC inhibition reduces NRP1 expression and SRC/FAK/ROCK1 pathway activity [40]. Additionally, HDAC1 promotes metastasis through SMO/Hedgehog activation via miR-326 suppression [41].

Conversely, HATs mediate lysine acetylation using acetyl-CoA, promoting transcription initiation [42]. KAT7, for instance, regulates osteosarcoma metastasis and immune responses through CCL3/JAK-STAT signaling and epithelial-mesenchymal transition (EMT) markers [43]. Similarly, HBO1 overexpression in osteosarcoma promotes tumor growth and migration [44]. The BET protein family, which recognizes acetylated

histones, shows oncogenic relevance [45], with NHWD-870 improving chemosensitivity via GP130/STAT3 inhibition [46]. BRD4 further modulates lipid metabolism and ferroptosis through ACSL3 splicing [47]. While these findings suggest histone acetylation's involvement in osteosarcoma progression, current research remains fragmented, focusing on individual histone acetylation modification-related protein (HAMRP) or specific sites. Notably, no integrated multi-omics studies have systematically examined HAMRPs' effects on immune infiltration and clinical outcomes in osteosarcoma.

Our study integrates bulk and single-cell osteosarcoma transcriptomics to characterize HAMRPs. We identified two acetylation patterns correlating strongly with immune-inflamed and immune-desert phenotypes. Focusing on metastatic mechanisms, we elucidated ASH1L's role in migration and EMT. The resulting ASH1L-based risk model effectively captures tumor heterogeneity while demonstrating prognostic value. This comprehensive HAMRP analysis may enable better outcome prediction and precision therapy.

2 Methods

2.1 Data sources

A thorough examination of osteosarcoma cohorts was performed using two publicly available databases: the GEO database (https://www.ncbi.nlm.nih.gov/geo/) and the TARGET database (https://www.cancer.gov/ccg/research/genome-sequencing/target). The GSE21257 cohort included 53 osteosarcoma patients with comprehensive follow-up and sequencing data for survival analysis. The TARGET cohort included 85 osteosarcoma patients with clinically documented data and matching bulk RNA-seq information. Bulk RNA-seq data were normalized using transcripts per kilobase million (TPM) and then log2-transformed to represent gene expression levels. For duplicate data, the mean RNA expression level was used. The gene expression matrices were integrated to form an osteosarcoma meta-cohort of 138 samples. To mitigate any potential bias, the "SVA" package was employed for correction. We performed differential gene expression analysis using the limma-voom pipeline on log2(TPM + 1) transformed data. Lowly expressed genes were first filtered. The voom transformation with precision weights was applied to model mean-variance relationships, followed by linear modeling with empirical Bayes moderation. P-values were adjusted using the Benjamini-Hochberg method (FDR < 0.05).

2.2 Determination of different patterns by consensus clustering analysis

The HAMRP gene list was compiled from published literature (see supplementary Table S1) [21, 48, 49]. To identify prognosis-related HMARPs, univariate Cox regression was implemented to screen gene lists using the "survival" package. The presence of a hazard ratio (HR) greater than 1 signifies a more unfavorable prognosis, while an HR less than 1 denotes a more favorable prognosis. Furthermore, unsupervised consensus clustering with the k-means clustering algorithm was performed for 1000 replicates to identify potential histone acetylation modification patterns in osteosarcoma. This analysis was facilitated by the "ConsensusClusterPlus" package. The optimal cluster count was determined through the use of cumulative distribution function (CDF) and consensus matrices, with the cluster number (k) ranging from two to ten. Kaplan-Meyer (KM) analysis was executed with the utilization of the "survival" and "survminer" packages to ascertain

the overall survival (OS) of varied histone acetylation modification patterns. Principal component analysis (PCA) was conducted to ascertain the heterogeneity among distinct histone acetylation modification patterns. Subsequently, the expression levels of prognostically relevant HAMRPs in various patterns were analyzed using the limma-voom pipeline.

2.3 Immune landscape analysis and biological feature analysis of histone acetylation modification patterns

The ESTIMATE algorithm was employed to assess variations in the tumor microenvironment (TME) across different histone acetylation modification patterns, while the ssGSEA algorithm quantified tumor-infiltrating immune cells (TICs) within these patterns. We employed the c2.cp.kegg_medicus.v2023.2.Hs.symbols.gmt marker gene sets for gene set variation analysis (GSVA) to elucidate the distinct functions and enrichment pathways associated with various histone acetylation modification patterns. We conducted gene set enrichment analysis (GSEA) with marker gene sets (c6.all.v2023.2.Hs.symbols.gmt) to investigate oncogenic signaling across various histone acetylation modification patterns. A statistically significant result was defined as an adjusted P value less than 0.05.

2.4 Subcellular localization and single-cell transcriptome analysis

TISCH2 (http://tisch.comp-genomics.org/) was utilized to analyze single-cell RNA sequencing data from the GSE162454 cohort. The single-cell mRNA expression of HAMRPs in immune-infiltrating and osteosarcoma cells was evaluated following the elimination of inter-sample batches, the uniform annotation of cell types, and the identification of malignant cells. Additionally, subcellular localization was determined using immunofluorescence images from the Human Protein Atlas (HPA, https://www.proteinatlas.org/, HPA accession: HPA004806). Composite images were generated by merging individual organelle marker channels (ASH1L, ER, DAPI, etc.), with splices reflecting natural interfaces between distinct fluorescent signals.

2.5 ASH1L-derived risk stratification system establishment and validation

The limma-voom pipeline was employed to identify differentially expressed genes (DEGs) between ASH1L high- and low-expression subgroups. Significant DEGs (adjusted p-value ≤ 0.05) were subsequently analyzed through Gene Ontology (GO) and Kyoto Encyclopedia of Genes and Genomes (KEGG) pathway enrichment analyses.

Using the "caret" package, the osteosarcoma meta-cohort was randomly partitioned into training and validation sets in equal proportions, with the training cohort utilized for model development and both test and combined cohorts employed for validation. To construct the ASH1L-derived prognostic index (ADPI), we first performed univariate Cox regression to evaluate the prognostic impact of the DEGs identified above, followed by LASSO regression for feature selection and multivariate Cox analysis to determine the final gene set and their respective coefficients. The ADPI score was calculated as the sum of each gene's expression level multiplied by its corresponding coefficient (ADPI score = Σ(coefi $\times$ Expi)).

Survival outcomes across different ADPI score groups were compared using Kaplan-Meier analysis, while the predictive accuracy of the ADPI was assessed across all cohorts

through time-dependent receiver operating characteristic (ROC) curve analysis, performed using the "timeROC" package.

2.6 Clinical correlation analysis

Cox regression analysis assessed the ADPI score's role as an independent prognostic factor. Correlations between ADPI score and clinicopathologic characteristics were analyzed using Kruskal-Wallis and Wilcoxon rank-sum tests. Kaplan-Meier survival analyses were conducted across various subgroups based on age (≤ 18 and > 18 years), sex (female and male), and metastatic status (metastatic and non-metastatic).

2.7 Cell lines

The human osteoblast cell (hFOB1.19) and the osteosarcoma cell lines (MG63 U2OS, and MNNG/HOS) were sourced from the China Center for Type Culture Collection (Shanghai, China). Osteosarcoma cell lines were cultured in a medium with 10% fetal bovine serum and 100 U/ml penicillin/streptomycin at 37 °C with 5% CO2. The hFOB1.19 cells were maintained at 33.5 °C with 5% carbon dioxide. Prior to freezing, authentication of these cells was conducted using STR identification.

2.8 Quantitative real-time reverse transcription-PCR (qRT-PCR)

RNA was isolated using RNA-easyTM reagent from Vazyme Biotech Co., Ltd., Nanjing, China, followed by cDNA synthesis using a reverse transcription kit (Yeasen, China). QRT-PCR analysis was conducted using the SYBR Green Master Mix (Takara, China) on a Bio-Rad CFX96 instrument (USA). Relative gene expression was calculated using the $2-\Delta\Delta CT$ method, with β-actin serving as the internal control. Supplementary Table S2 provides primer sequences for relevant genes.

2.9 Plasmid construction and transfection

RiboBio (Guangzhou, China) synthesized shRNA sequences for ASH1L for gene downregulation, as detailed in supplementary Table S3. GenePharma (Suzhou, China) created plasmids that overexpress ASH1L and an empty vector. Transfection was performed using Lipofectamine 3000 (Invitrogen, USA) and assessed 24–48 h later using qRT-PCR or western blot (WB).

2.10 Western blot assay

The cells were lysed in RIPA lysis buffer with protease and phosphatase inhibitors, all from Beyotime, China. Proteins were separated using 8–10% SDS-PAGE and subsequently transferred to a PVDF membrane (Millipore, USA). The membranes were then blocked using rapid blocking liquid (NCM Biotech, Suzhou, China) and incubated with the appropriate primary antibodies at 4 °C overnight. The blots were then subjected to an enhanced chemiluminescence reagent (NCM Biotech, Suzhou, China). Antibody against mTOR (66888-1-Ig), p-AKT (66444-1-Ig), E-cadherin (60335-1-Ig), N-cadherin (66219-1-Ig), p-mTOR (67778-1-Ig), AKT (60203-2-Ig), β-actin (66009-1-Ig), and vimentin (60330-1-Ig) were obtained from Proteintech (Wuhan, China). ASH1L antibody (ab50981) was purchased from Abcam (Shanghai, China). Band intensities were quantified using Image J (v.1.53), normalized to β-actin. Data represent mean ± SEM ($n = 3$ independent experiments).

2.11 Wound healing assay

Before the confluence of osteosarcoma cells reaches 90%, a scratch is produced in each well of the plate with a 200 μL sterile pipette tip.Subsequently, the medium was replaced with serum-free medium. Photographs of each wound were taken at 0, 24, and 48 h after changing the culture medium.The migration speed was determined using the scratch width.

2.12 Transwell assay

Osteosarcoma cells were transfected and re-suspended in a serum-free medium. A single-cell suspension was then seeded into each upper chamber of 24-well transwell inserts (JET Biofil, China) with or without matrix to assess the cells' migration or invasion capabilities. After 16 h of culture, the bottom of each transwell insert was washed with PBS, then fixed with 4% paraformaldehyde and stained with 0.1% crystal violet.

2.13 Statistical analysis

Data analysis was conducted using R4.3.0. Data were reported as mean ± standard deviation for at least three separate experiments. Comparisons were conducted using either Student's t-test or one-way ANOVA. $^{*}P < 0.05$; $^{**}P < 0.01$; $^{***}P < 0.001$; NS no significance.

3 Results

3.1 Prognostic significance and subtype identification of HAMRPs in osteosarcoma

We initially conducted an analysis of the association between HAMRPs and outcomes in conjunction with the TARGET and GEO cohorts. Univariate Cox regression analysis identified eight HAMRPs significantly influencing osteosarcoma patient prognosis (Fig. 1A). As an indicator of good prognosis, SP140 exhibited a substantial positive correlation with SP110, yet a pronounced negative correlation with indicators of poor prognosis, encompassing ASH1L, ZMYND11, HDAC4, and SIRT1 (Fig. 1B). The chromosomal location of the aforementioned prognosis-related HMARPs is displayed in Fig. 1C.

Osteosarcoma patients were grouped using unsupervised clustering to examine the influence of HAMRPs on different molecular subtypes. Two distinct histone acetylation modification patterns, labeled HAMPcluster C1 and HAMPcluster C2, were identified (Fig. 1D-F). The HAMPcluster C1 exhibited a substantial survival benefit, as evidenced by Fig. 1G. In addition, PCA analysis further confirmed a clear separation between HAMPcluster C1 and HAMPcluster C2 (Fig. 1H). Subsequent investigations into the transcriptional profiles of HAMRPs between two distinct phenotypes revealed that HAMRPs identified as favorable indicators (comprising SP140 and SP110) demonstrated remarkably elevated expression levels in HAMPcluster C1 (Fig. 1I). By contrast, HAMRPs with adverse prognostic potential (e.g., ASH1L, ZMYND11, SMARCA2, HAT1, HDAC4, and SIRT1) exhibited significantly higher expression in HAMPcluster C2 (Fig. 1I).

3.2 Distinct TME characteristics in the two histone acetylation modification patterns

CIBERSORT analysis identified significant differences in naive B cells, memory B cells, plasma cells, CD8 + T cells, regulatory T cells (Tregs), gamma delta T cells, macrophages, and monocytes across various histone acetylation modification patterns (Fig. 2A-B).

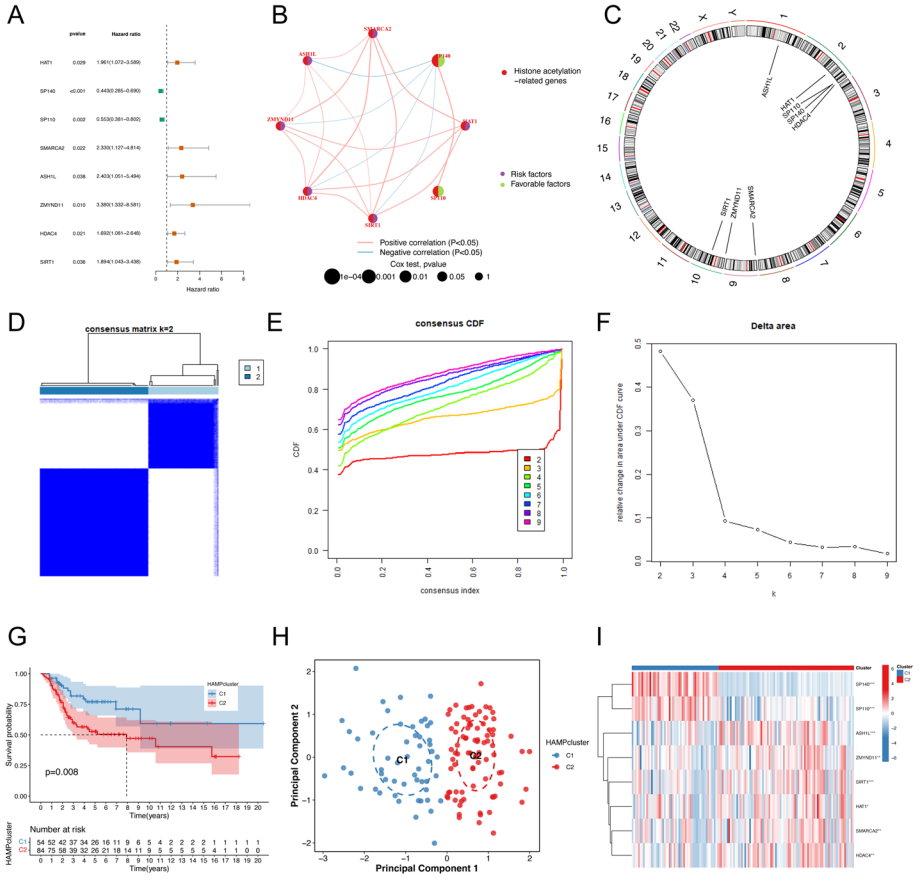

Fig. 1 Determination of histone acetylation modification patterns in osteosarcoma. **(A)** Prognosis-related HMARPs in osteosarcoma filtered by univariate Cox regression. **(B)** Interactions among HAMRPs in osteosarcoma, with red and blue lines denoting positive and negative correlations, respectively. **(C)** Location of prognosis-related HMARPs on different chromosomes. **(D)** Unsupervised clustering of prognosis-related HMARPs in osteosarcoma cohort and consensus matrices for k = 2. **(E)** The cumulative distribution function plot of consensus clustering at k = 2–9. **(F)** The delta plot assessing the change in area under the CDF curve. **(G)** Kaplan-Meier analysis for assessing overall survival in two histone acetylation modification patterns. **(H)** Principal component analysis demonstrating the distribution of two histone acetylation modification patterns in osteosarcoma. **(I)** The expression of prognosis-related HMARPs between two distinct histone acetylation modification patterns

Subsequent assessment of the overall variation in TME using the ESTIMATE algorithm revealed that HAMPcluster C1 exhibited the higher immune score and the lower tumor purity, indicative of a superior immune response (Fig. 2C). Conversely, HAMPcluster C2 demonstrated the opposite characteristics (Fig. 2C).

The application of the ssGSEA method revealed that the HAMPcluster C1 exhibited augmented immune cell infiltration, including dendritic cells (DCs), activated DCs, CD8 + T cells, natural killer (NK) cells, plasmacytoid DCs, T follicular helper cells (Tfh), Th1 cells, macrophages, neutrophils, Th2 cells, tumor-infiltrating lymphocytes (TILs), Tregs, and T helper cells (Fig. 2D). These findings align with the immunoinflammatory phenotype characteristics. Simultaneously, the HAMPcluster C2 pathway activity was suppressed, affecting checkpoint, Type I IFN Response, APC co-inhibition, APC co-stimulation, cytokine-cytokine receptor, cytolytic activity, human leukocyte antigen (HLA), inflammation-promoting, MHC class I, para-inflammation, T cell co-inhibition, and T cell co-stimulation (Fig. 2D). Accordingly, HAMPcluster C2 was classified as an immune-desert phenotype characterized by immunosuppression and minimal immune

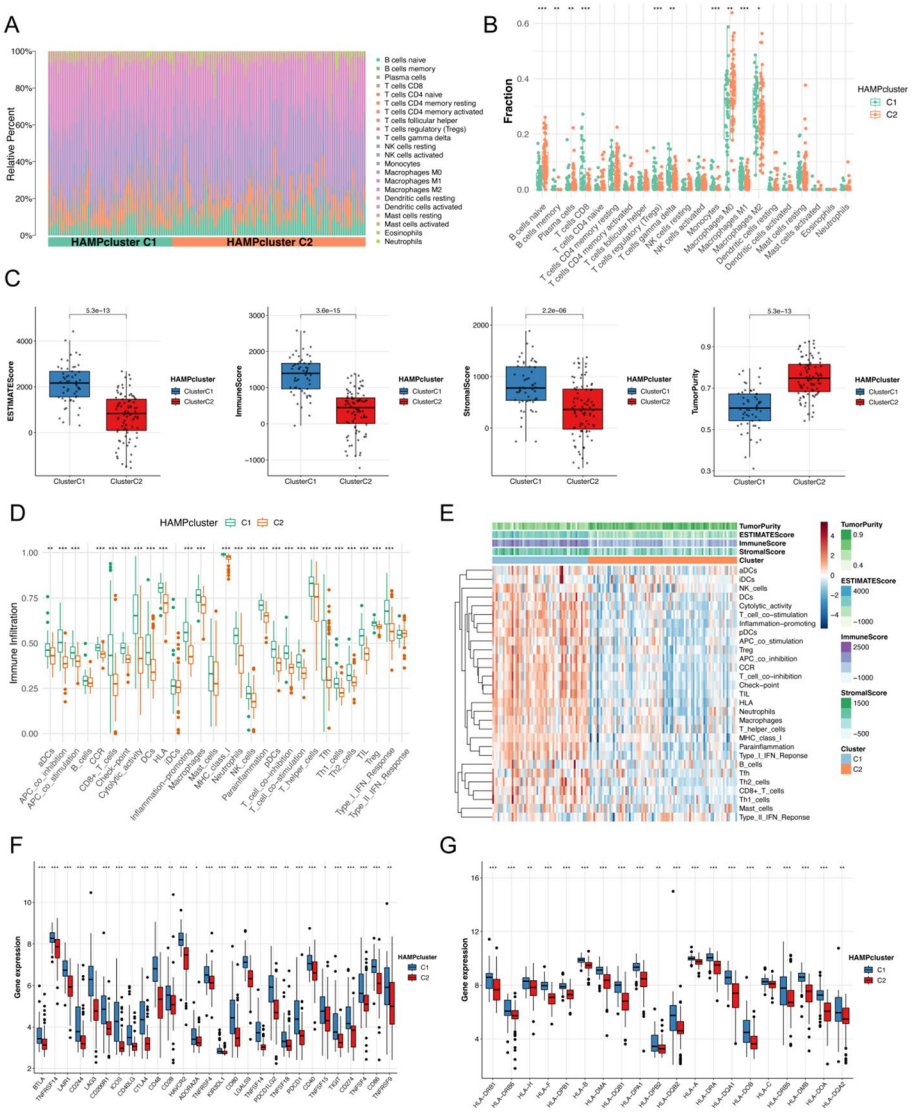

Fig. 2 Characterization of the immune landscape for each histone acetylation modification pattern. **(A-B)** The proportion of immune-infiltrating cells in two histone acetylation modification patterns analyzed by CIBERSORT. **(C)** Discrepancies in overall immune status between HAMPcluster C1 and C2 samples. **(D)** Differences in immune cell infiltration and immune-activated pathways between HAMPcluster C1 and C2 analyzed by ssGSEA. **(E)** Heatmap for visualization of differences in the immune score, stromal score, ESTIMATE score, tumor purity, immune cells, and function in distinct histone acetylation modification patterns. **(F-G)** Expression patterns of immune checkpoints **(F)** and major histocompatibility complex molecules **(G)** in distinct histone acetylation modification patterns

cell infiltration, consistent with its low probability of survival (Fig. 2A-E). In addition, HAMPcluster C2 also had attenuated expression of immune checkpoint genes (ICGs) and major histocompatibility complex (MHC) molecules, with particularly pronounced downregulation of LAG3, CTLA4, HAVCR2, CD48, LGALS9, HLA – DQB1 and HLA – DPA1 (Fig. 2F-G). In general, HAMPcluster C2 exhibited reduced immune cell infiltration and lower expression of ICGs compared to another cluster.

3.3 Distinct clinicopathologic features and functional annotations in the two histone acetylation modification patterns

The relationship between histone acetylation modification patterns and clinicopathologic characteristics, such as age, gender, and metastasis, was further investigated. A higher proportion of patients with metastatic osteosarcoma was observed in HAMPcluster C2 compared to HAMPcluster C1 (Fig. 3A). Notably, histone acetylation modification patterns were found to be independent of age but correlated with gender, with a higher proportion of male patients in HAMPcluster C2 (Fig. 3B-C). GSVA enrichment analysis was performed to assess the biological characteristics and activities of the two distinct histone acetylation modification patterns. As illustrated in Fig. 3D, HAMPcluster C1 demonstrated a marked enrichment in biosynthesis, apoptotic, and JAK-STAT pathways, including NAD biosynthesis, bile acid biosynthesis, extrinsic apoptotic pathway, and cytokine JAK-STAT signaling pathway. A GSEA analysis using C6 oncogenic signature gene sets was performed to investigate the link between histone acetylation modification patterns and carcinogenesis pathways. The gene signatures representing E2F3-activated (E2F3_UP.V1_UP) and KRAS-activated (KRAS.KIDNEY_UP.V1_UP) were particularly enriched in HAMPcluster C2 (Fig. 3E). Conversely, HAMPcluster C1 was associated with the STK33-activated oncogenic signatures (STK33_SKM_UP, STK33_NOMO_UP, and STK33_UP) (Fig. 3F).

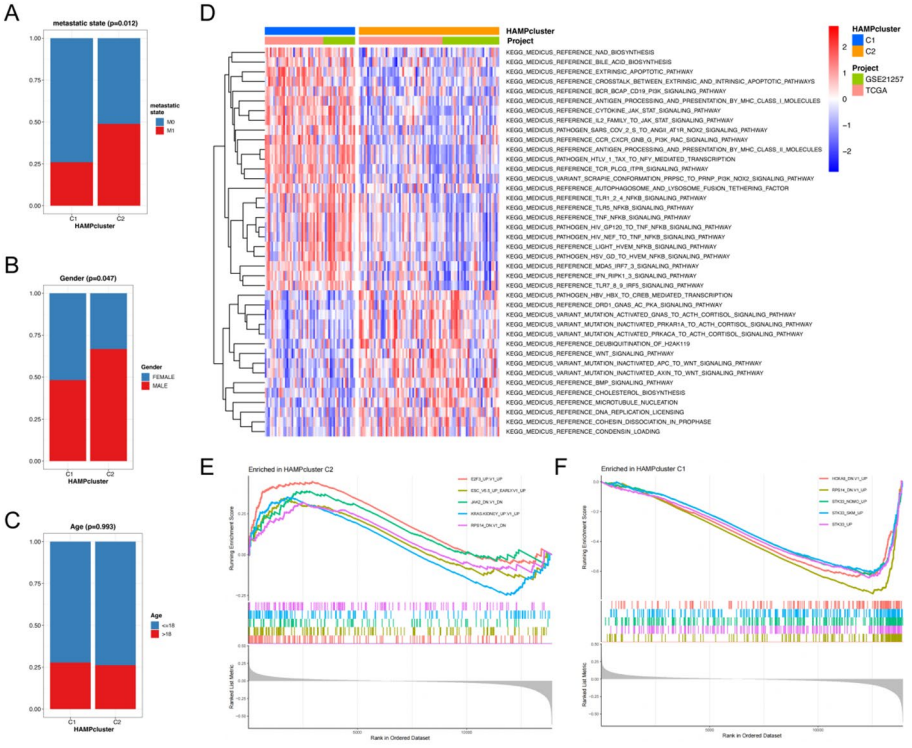

Fig. 3 Characterization of the clinical parameters and potential biological mechanisms for each histone acetylation modification pattern. **(A-C)** Clinical correlation analysis between histone acetylation modification patterns and clinical information including metastatic status **(A)**, gender **(B)**, age **(C)**. **(D)** GSVA enrichment analysis showing distinct activation states of biological pathways in distinct histone acetylation modification patterns. **(E-F)** GSEA enrichment analysis of HAMPcluster C1 and C2 using C6 oncogenic signature gene sets

3.4 Relationship between HAMRPs and clinicopathologic features

This study aimed to investigate the association between prognosis-related HMARPs and clinicopathological characteristics in osteosarcoma. However, no substantial disparities were identified in the expression of the eight prognosis-related HMARPs among various clinical subgroups of osteosarcoma, including different age stratifications and between male and female patients (Supplementary Fig. 1).

Metastasis continues to significantly hinder the improvement of prognosis in osteosarcoma patients [50, 51]. While no significant associations were found between the expression of six of the prognosis-related HMARPs and metastasis, ASH1L and SP140 stood out in our analysis (Fig. 4A, Supplementary Fig. 2). We observed that ASH1L expression was significantly higher in metastatic osteosarcoma cases, while SP140 expression was elevated in non-metastatic cases (Fig. 4A). This differential expression pattern suggested a potential role for ASH1L in osteosarcoma metastasis.

Subsequently, patients were stratified according to ASH1L and SP140 expression levels. Consistently, KM survival analysis demonstrated that patients with higher SP140 expression exhibited significantly prolonged overall survival (OS) ($P = 0.008$), while higher ASH1L expression was associated with poorer OS ($P = 0.011$) (Fig. 4B).These findings further supported the hypothesis that ASH1L plays a significant role in osteosarcoma prognosis.

Furthermore, we explored the expression of ASH1L and SP140 at the single-cell level (Fig. 4C). ASH1L was more abundantly expressed in malignant cells compared to SP140,

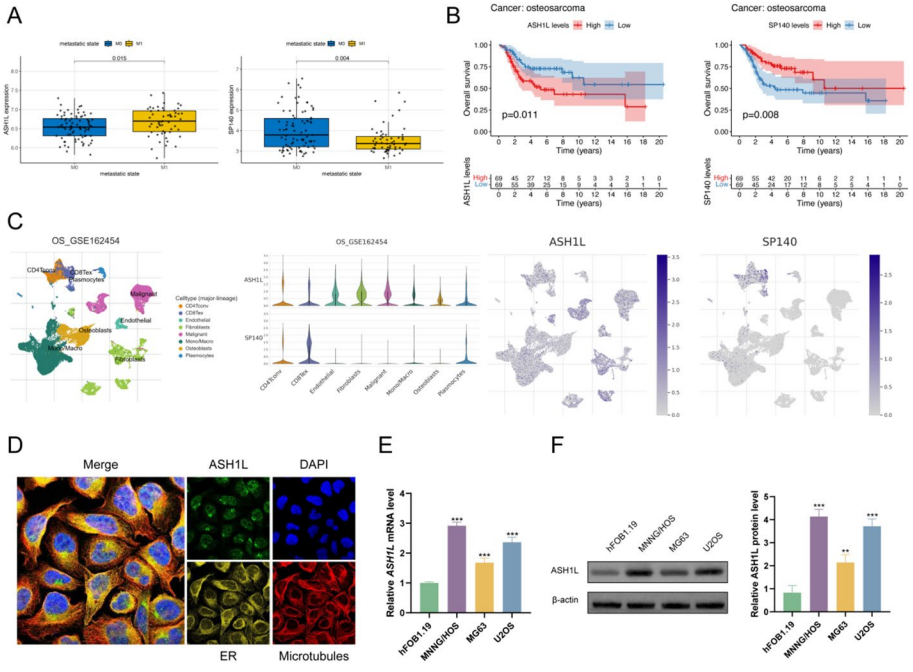

Fig. 4 Screening ASH1L as a potential aggressive marker for osteosarcoma. **(A)** ASH1L expression levels were elevated in patients with metastatic osteosarcoma, while SP140 expression levels were attenuated in patients with metastatic osteosarcoma. **(B)** Kaplan-Meier analysis for assessing overall survival of osteosarcoma patients with different ASH1L or SP140 expression. **(C)** The expression distribution of ASH1L and SP140 in osteosarcoma and immune cell subpopulations at the single-cell level. Cell-type annotations were supplied by TISCH, and gene expression levels were visualized using UMAP plots. **(D)** Immunofluorescence analysis of ASH1L subcellular localization in U2OS cells. **(E)** Expression of ASH1L in hFOB1.19 cells and osteosarcoma cells detected by qRT–PCR. **(F)** Western blot and quantitative analysis of ASH1L protein levels in hFOB1.19 cells and osteosarcoma cells

reinforcing the idea that ASH1L may be involved in the malignant progression of osteosarcoma (Fig. 4C).

Given the extensive literature on the role of SP140 in osteosarcoma [52–55], our subsequent focus shifted to investigating the specific function of ASH1L in osteosarcoma and its underlying mechanisms. We first characterized the subcellular localization and expression of ASH1L in osteosarcoma using HPA database (accession number: HPA004806). Immunofluorescence staining revealed that ASH1L was predominantly expressed in the nucleoplasm and the Golgi apparatus (Fig. 4D, Supplementary Fig. 3). Additionally, the expression level of ASH1L in osteosarcoma cell lines was significantly elevated compared to that in control osteoblasts, as detected by qRT-PCR and Western blotting (Fig. 4E-F).

3.5 ASH1L modulates osteosarcoma metastasis via EMT

ASH1L's role in osteosarcoma metastasis was further investigated by stable knockdown of ASH1L in two osteosarcoma cell lines (Fig. 5A-B). As demonstrated in Fig. 5C-D, osteosarcoma cells with ASH1L downregulation exhibited diminished invasion and migration capabilities compared to the control cells by Transwell assays. In accordance with these observations, the scratch wound healing assays revealed reduced cell migration ability following ASH1L silencing in MNNG/HOS and MG63 cells (Fig. 5E). EMT has been identified as a hallmark of cancer as well as a pivotal factor in tumor metastasis [56, 57]. Therefore, we analyzed EMT marker expression in osteosarcoma cells after ASH1L knockdown. The results demonstrated that suppression of ASH1L enhanced the

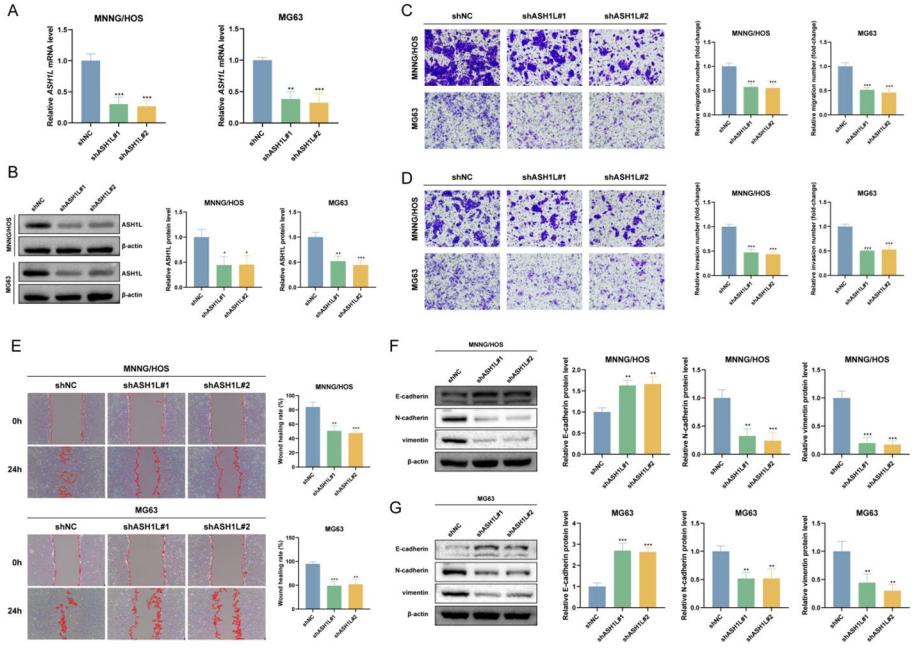

Fig. 5 ASH1L knockdown impairs osteosarcoma metastasis and EMT. **(A-B)** Validation of ASH1L downregulation in MNNG/HOS and MG63 cells by qRT-PCR **(A)** and Western blot **(B)**. **(C)** The impaired cell migration of osteosarcoma cells after ASH1L silencing in transwell assays. **(D)** The impaired cell invasion of osteosarcoma cells after ASH1L silencing in transwell assays. **(E)** The impaired cell migration of osteosarcoma cells after ASH1L silencing in scratch wound healing assays. **(F)** Western blot and quantitative analysis of EMT marker expression levels in MNNG/HOS cells after silencing ASH1L. **(G)** Western blot and quantitative analysis of EMT marker expression levels in MG63 cells after silencing ASH1L

expression of epithelial markers (E-cadherin) and diminished the expression of mesenchymal markers (N-cadherin and vimentin) (Fig. 5F-G).

The qRT-PCR and WB results indicated the successful establishment of MNNG/HOS and MG63 cells overexpressing ASH1L (Fig. 6A-B). As anticipated, the proliferative and invasive capabilities of osteosarcoma cells transfected with the ASH1L overexpressing plasmid were considerably elevated (Fig. 6C-E). Furthermore, the expression levels of E-cadherin were reduced, while N-cadherin and Vimentin expression levels were increased (Fig. 6F-G). Consequently, these findings collectively indicate that ASH1L functions as a positive regulator of osteosarcoma metastasis.

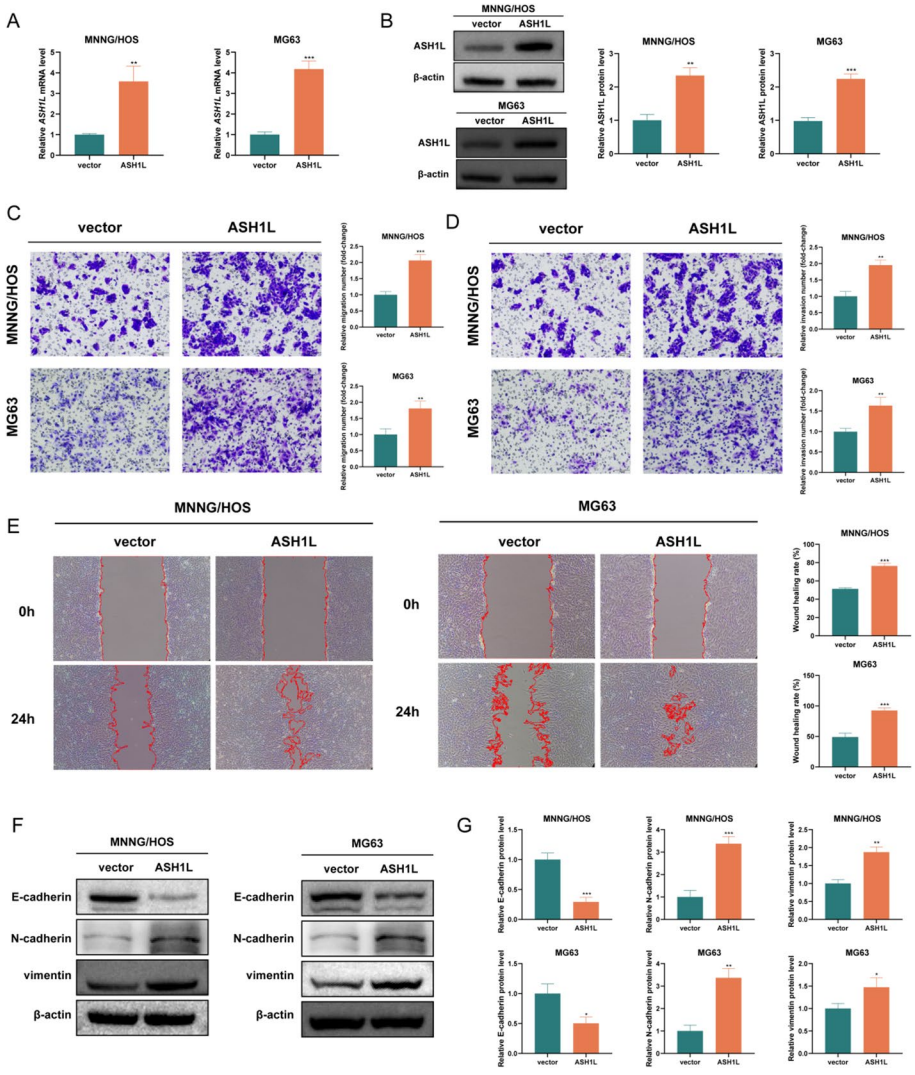

Fig. 6 ASH1L overexpression promotes osteosarcoma metastasis and EMT. **(A-B)** Validation of ASH1L overexpression in MNNG/HOS and MG63 cells by qRT-PCR **(A)** and Western blot **(B)**. **(C)** The enhanced cell migration of osteosarcoma cells after ASH1L overexpression in transwell assays. **(D)** The enhanced cell invasion of osteosarcoma cells after ASH1L upregulation in transwell assays. **(E)** The enhanced cell migration of osteosarcoma cells after ASH1L overexpression in scratch wound healing assays. **(F)** Western blot analysis was used to determine the expression levels of EMT markers after ASH1L upregulation. **(G)** Quantitative analysis of EMT marker expression levels in osteosarcoma cells after ASH1L overexpression

3.6 ASH1L affects AKT/mTOR signaling in osteosarcoma

We conducted GO, KEGG, and GSEA analyses to investigate the molecular mechanisms by which ASH1L enhances osteosarcoma cell migration and invasion. A total of 1722 DEGs were identified between patients with osteosarcoma exhibiting high and low expression of ASH1L (Supplementary Fig. 4). The DEGs were mainly associated with immune-related GO terms, such as MHC protein complex binding, T cell activation regulation, and immune receptor activity (Fig. 7A). With regard to the KEGG pathway, DEGs were predominantly implicated in osteoclast differentiation and rheumatoid arthritis (Fig. 7B). GSEA analysis indicated significant enrichment of the MTOR_UP.N4.V1_DN gene set in the low-ASH1L expression subgroup (Fig. 7C). Multiple molecular mechanisms facilitate EMT, and the AKT/mTOR signaling cascade represents a pivotal pathway modulating cancer metastasis and EMT process [58–60]. We therefore assayed the expression of phosphorylated AKT (p-AKT), AKT, phosphorylated mTOR (p-mTOR), and mTOR to explore the impact of ASH1L on AKT/mTOR activation in osteosarcoma cells. Consistent with the results of GSEA, the WB assay revealed

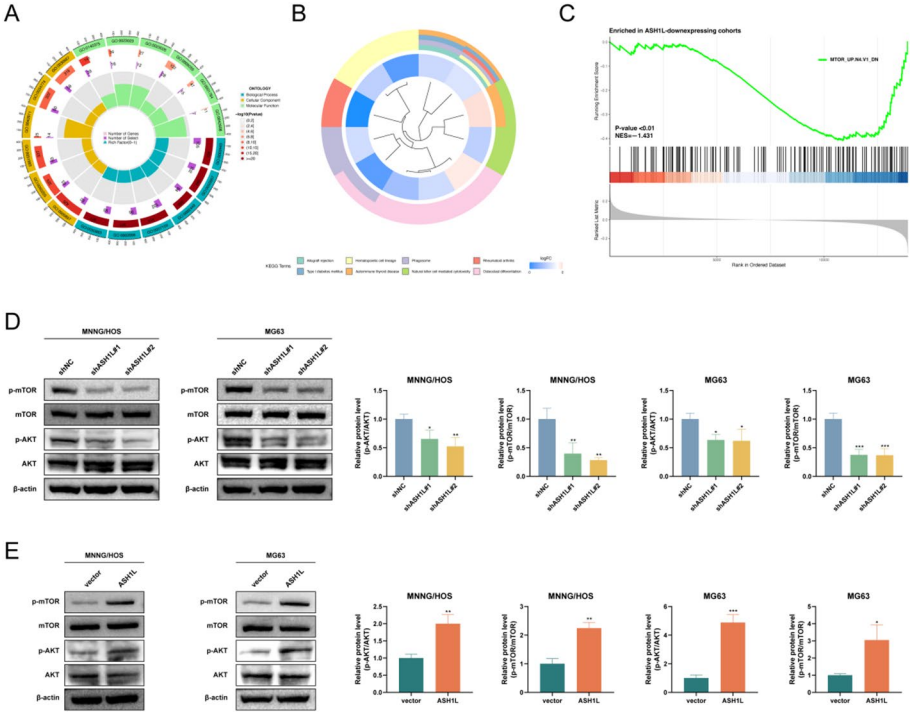

Fig. 7 ASH1L positively regulates AKT/mTOR pathway in osteosarcoma cells. **(A)** GO enrichment analysis of DEGs between high and low ASH1L expression groups, which includes the top 6 significantly enriched terms from each of the three GO categories: biological processes, including leukocyte mediated immunity (GO:0002443), positive regulation of cell activation (GO:0050867), lymphocyte mediated immunity (GO:0002449), leukocyte cell-cell adhesion (GO:0007159), positive regulation of leukocyte activation (GO:0002696), regulation of T cell activation (GO:0050863); molecular functions, including immune receptor activity (GO:0140375), MHC protein complex binding (GO:0023023), MHC class II protein complex binding (GO:0023026), electron transfer activity (GO:0009055), phosphotyrosine residue binding (GO:0001784), T cell receptor binding (GO:0042608); and cellular components, including external side of plasma membrane (GO:0009897), cytoplasmic vesicle lumen (GO:0060205), vesicle lumen (GO:0031983), MHC protein complex (GO:0042611), secretory granule lumen (GO:0034774), secretory granule membrane (GO:0030667). **(B)** KEGG enrichment analysis of DEGs between high and low ASH1L expression groups. **(C)** GSEA analysis showing that ASH1L expression is correlated with mTOR signaling pathway activity. **(D)** Western blot and quantitative analysis of p-AKT, AKT, p-mTOR, and mTOR expression levels in osteosarcoma cells with ASH1L silencing. **(E)** Western blot and quantitative analysis of p-AKT, AKT, p-mTOR, and mTOR expression levels in osteosarcoma cells with ASH1L overexpression

that ASH1L knockdown attenuated the phosphorylation of AKT and mTOR (Fig. 7D). Conversely, ASH1L overexpression augmented the protein expression of p-AKT and p-mTOR (Fig. 7E). Collectively, the above findings demonstrated that ASH1L promoted AKT/mTOR signaling and metastasis of osteosarcoma cells.

3.7 Predicting prognosis in osteosarcoma patients using the ASH1L-derived risk stratification system

In order to further refine the ASH1L-derived risk stratification system, univariate COX regression analysis was conducted to filter 371 OS-related DEGs (Fig. 8A). After the LASSO algorithm and multivariate Cox regression, 10 final candidate DEGs were screened to construct the ADPI for application to individual osteosarcoma patients (Fig. 8B-C). The formula of ADPI is as follows: ADPI score = (0.90109 × MYC) + (-2.46868 × SIGLEC11) + (-0.33500 × PRAME) + (-3.83926 × CASK) + (1.16010 × LYNX1) + (-3.07271 × USP9X)+ (-2.48589 × WDR53) + (-0.71537 × CACNA2D3) + (-0.57813 × CNR1) + (1.34005 × MCF2). The ADPI scores were calculated for each

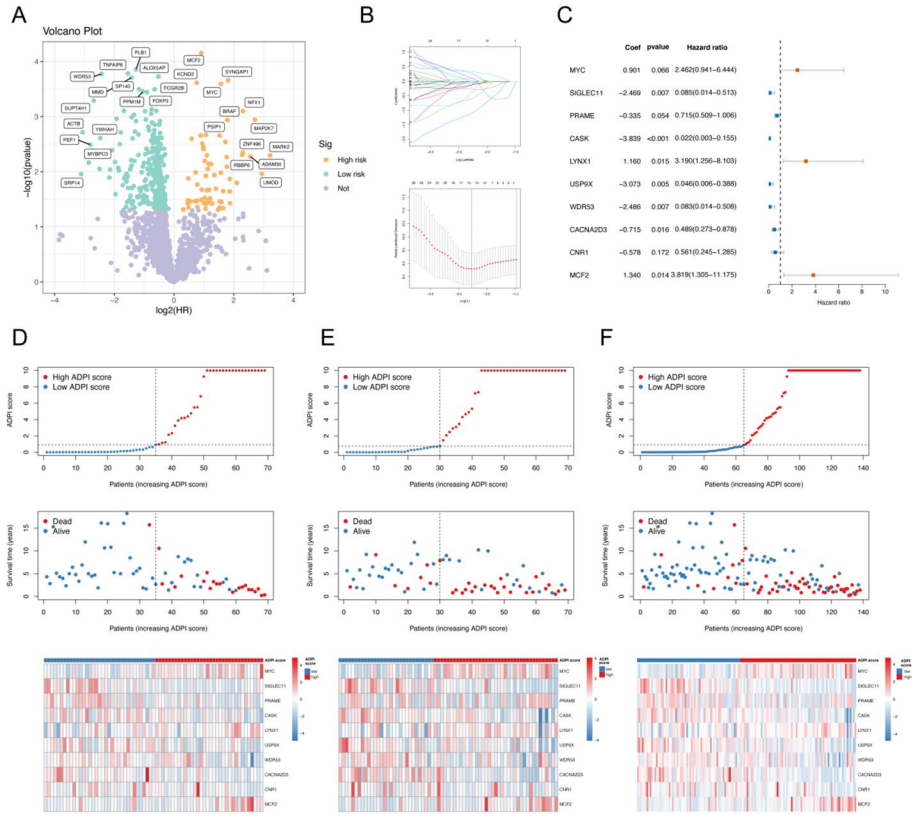

Fig. 8 Construction of the ASH1L-derived risk stratification system. **(A)** Volcano plot of univariate COX regression. The x-axis represents the magnitude of the effect size, in the form of HR. A HR greater than 1 suggests an increased risk, while a HR less than 1 suggests a protective effect. The y-axis represents the statistical significance of each variable. Points on the plot represent individual variables (DEGs). (B) Construction of the ASH1L-derived risk stratification system using LASSO regression analysis. Plot for the coefficients of LASSO regression (upper panel). Ten-fold cross-validation for LASSO regression to select the optimal penalty coefficient (lower panel). (C) Construction of the ASH1L-derived risk stratification system using multivariate Cox analysis in the training cohort from the meta-cohort. **(D)** Distribution of ADPI scores, survival status, and expression of hub DEGs in the training cohort from the meta-cohort. **(E)** Distribution of ADPI scores, survival status, and expression of hub DEGs in the validation groups from the meta-cohort. **(F)** Distribution of ADPI scores, survival status, and expression of hub DEGs in the entire cohort

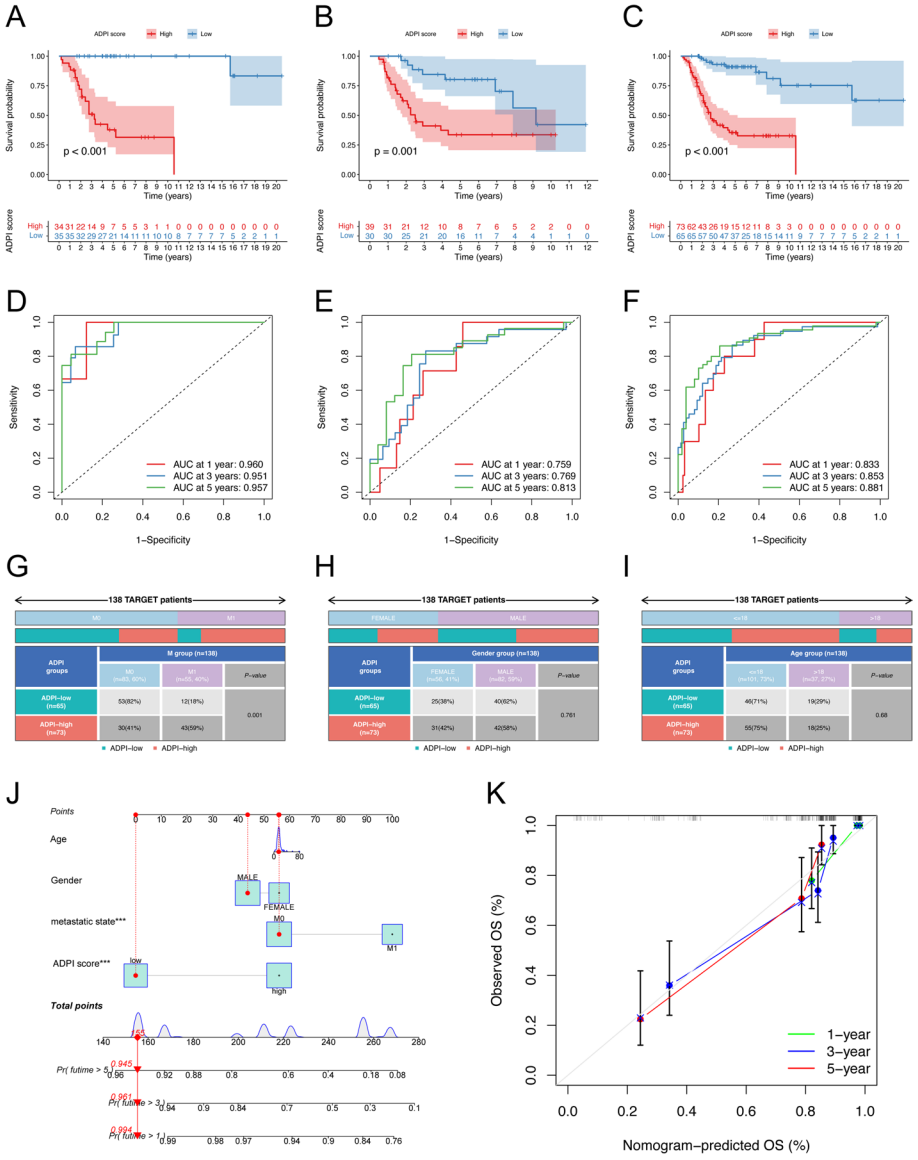

Fig. 9 Validation of the ASH1L-derived risk stratification system and the relationship between ADPI scores and clinical parameters. **(A-C)** Survival analysis of osteosarcoma patients with various ADPI scores in the training cohort **(A)**, validation cohort **(B)**, and entire cohort **(C)** from the meta-cohort. **(D-F)** ROC curves for osteosarcoma patients with various ADPI scores in the training cohort **(D)**, validation cohort **(E)**, and entire cohort **(F)** from the meta-cohort. **(G)** Associations between ADPI scores and metastatic status of osteosarcoma in the meta-cohort. **(H)** Associations between ADPI scores and gender of osteosarcoma in the meta-cohort. **(I)** Associations between ADPI scores and age of osteosarcoma in the meta-cohort. **(J)** A nomogram that integrates ADPI score and other clinical parameters of osteosarcoma in the meta-cohort. **(K)** The calibration curve of the nomogram

patient in both the training and test cohorts and patients were subsequently categorized into high- and low-risk groups (Fig. 8D-F). A notable heterogeneity in survival time was found between osteosarcoma patients with elevated and reduced ADPI scores (Fig. 9A-C). In all cohorts, osteosarcoma patients with higher ADPI scores exhibited a higher mortality rate (Fig. 9A-C). The AUC values of 0.960, 0.951, and 0.957 at 1, 3, and 5 years, respectively, confirmed the excellent potential of the ASH1L-derived genetic prognostic index in assessing the outcomes (Fig. 9D). Similar results were obtained for the validation and the entire cohort, with AUCs exceeding 0.7 (Fig. 9E-F). The results suggest that

the ASH1L-derived risk stratification system could be a useful tool for predicting clinical outcomes. Subsequent analysis of age, gender, and metastatic status across scoring subgroups revealed a significantly lower proportion of osteosarcoma metastases in the low ADPI scoring group (Fig. 9G-I). Furthermore, elevated ADPI scores were observed to potentially contribute to shorter OS times in various clinical subgroups of osteosarcoma, including patients aged above or below 18 years, patients with metastatic osteosarcoma, patients with non-metastatic osteosarcoma, male patients, and female patients (Supplementary Fig. 5). Finally, a nomogram was developed to predict outcomes in osteosarcoma patients, integrating clinicopathologic characteristics for easy calculation of individual survival probabilities (Fig. 9J). Calibration curve analysis confirmed that the nomogram's predictions were proximate to the observed outcomes (Fig. 9K). These findings suggest that ADPI could be a supplementary tool for risk stratification in osteosarcoma clinical management.

4 Discussion

Osteosarcoma, a highly aggressive bone cancer primarily affecting long bones and occasionally craniofacial regions, remains challenging to treat, particularly in metastatic cases [61–63]. Despite improved 5-year survival rates (~ 75%) for localized disease with surgery and chemotherapy, outcomes for metastatic osteosarcoma remain poor [64, 65]. Thus, understanding the molecular drivers of metastasis is critical for developing targeted therapies. Recent studies highlight histone acetylation modifiers as key players in cancer progression, making them attractive therapeutic targets [66–69]. Our study comprehensively explores histone acetylation modification patterns, their prognostic significance, clinical relevance, and impact on the immune landscape in osteosarcoma.

Osteosarcoma's biological heterogeneity contributes to variable treatment responses and disease outcomes [70, 71]. Using unsupervised clustering, we identified two distinct histone acetylation modification patterns with divergent prognoses and immune phenotypes. HAMPcluster C2, associated with higher tumor purity and shorter overall survival, contrasts with HAMPcluster C1, which exhibits higher immune infiltration and better outcomes. This suggests that immune activity within the TME influences prognosis.

The interaction between tumors and immune cells within the TME is increasingly recognized as a crucial factor in cancer progression and response to therapy [72–81]. Osteosarcoma is composed not only of malignant cells but also of infiltrating immune cells, cancer-associated stromal cells, and extracellular matrix components [82]. Our ssGSEA analysis revealed significant differences in immune cell infiltration (e.g., CD8 + T cells, macrophages, NK cells, and Tregs) between the two clusters. CD8 + T cells, known for their antitumor effects via IFN-γ and granzyme B production [83], exist in functionally diverse subsets (Tc1, Tc2, Tc22) that shape immune responses [84]. Similarly, NK cells modulate innate and adaptive immunity through cytokine secretion [85]. These TICs recruited into the TME exert pro- or antitumor functions and could profoundly influence tumor biology and antitumor immunological state [86]. These findings explain why HAMP cluster C1—with enhanced immune activation—correlates with better survival, offering potential insights for immunotherapeutic strategies. Immune checkpoint inhibitors (ICIs) hold promise but face challenges due to tumor heterogeneity and dynamic immune checkpoint gene (ICG) expression [87–89]. Moreover, a possible

resistance mechanism to ICIs is the abnormal HLA antigen presentation pathway [90]. Downregulation of HLA serves as an immune evasion mechanism employed by tumors [91]. Our investigation revealed that the expression levels of ICGs and MHC molecules could be effectively discriminated in the osteosarcoma patient population according to diverse HAMPs. In summary, the analysis of HAMPs could provide valuable insights into the TIME of osteosarcoma patients, potentially aiding in the development of personalized immunotherapy.

In order to identify potential therapeutic targets, we systematically evaluated all HAMRPs used in the initial unsupervised clustering by clinical correlation analysis and Kaplan-Meier survival assessment. Our investigation showed that among all analyzed HAMRPs, ASH1L expression was elevated in metastatic osteosarcoma cases and was strongly associated with poorer overall survival. Furthermore, single-cell genomics showed that ASH1L was more abundantly expressed in malignant cells compared to SP140. These results suggest that ASH1L may play a crucial role in osteosarcoma carcinogenesis. ASH1L belongs to the trithorax-group proteins, which are essential for epigenetic gene activation mechanisms and was first identified and cloned by the Nakamura group in 2000 [92–94]. Located at cytogenetic band 1q22, ASH1L is a histone methyltransferase that contains four AT hooks, an SET structural domain, a PHD finger motif, a bromoadjacent homology domain, and a bromodomain [95, 96]. Its bromodomain enables it to specifically bind to certain chromatin or protein targets, providing flexible regulation of its activity [93]. Furthermore, ASH1L specifically occupies the transcribed regions of active genes [95].

Several recent studies have demonstrated significant associations between ASH1L and immune infiltration patterns. Notably, ASH1L has been implicated in establishing an immunosuppressive microenvironment in hepatocellular carcinoma (HCC) by modulating the expression of zonula occludens-1, a critical tight junction protein [97]. Xia et al. discovered that ASH1L regulates induced Treg polarization and T cell autoimmunity through direct targeting of the Smad3 promoter and enhancing local H3K4 trimethylation [98]. Furthermore, ASH1L exerts its immunoregulatory effects through SET domain-dependent H3K4 methylation at the Tnfaip3 promoter, epigenetically activating transcription of A20 - a critical ubiquitin-editing enzyme [99]. This epigenome-immunome interplay highlights ASH1L as a potential therapeutic target for autoimmune disorders characterized by IL-6 dysregulation. In experimental autoimmune uveitis models, stabilization of ASH1L mRNA was shown to effectively suppress pathogenic Th17 cell responses [100]. Additionally, ASH1L-mediated histone modifications at the Elk3 promoter enhance chromatin accessibility and initiate Elk3 transcription, thereby driving group III innate lymphoid cell differentiation [101].

In our study, ASH1L exhibited elevated expression levels in all three osteosarcoma cell lines, with a predominant localization in the nucleoplasm and the Golgi apparatus. Previous studies have similarly shown that ASH1L is aberrantly expressed in various cancer types, contributing to malignancy and poor prognosis [96, 102–106]. Ding et al. confirmed the presence of ASH1L mutations and high levels of amplification in bladder cancer [107]. Demelash et al. observed that ASH1L altered Cdk5/p35 pathway activity in lung adenocarcinoma, contributing to the acquisition of highly metastatic and invasive features [108]. Overexpression of miR-142–3p in thyroid follicular adenomas acted as a tumor suppressor by significantly downregulating ASH1L and MLL1,

restoring thyroid-specific HOXB3 gene expression [109]. Additionally, ASH1L has been shown to trigger uncontrolled and persistent expression of HOXA9/A10 during normal myeloid differentiation, a process that contributes to leukemogenesis [110]. Zhu et al. demonstrated that ASH1L retains the histone H3K36 dimethylation mark and promotes the recruitment and stabilization of the oncogene MLL on chromatin, thereby inducing leukemogenesis [111]. Sustained activation of the ASH1L-AS1-ASH1L axis increased genome-wide H3K4me3 modification levels and modulated NME1-mediated RAS signaling in gastric cancer [96]. It is hypothesized that, due to the complexity of molecular mechanisms, ASH1L may have distinct functions in different cancers. However, the underlying molecular mechanisms of ASH1L in osteosarcoma remain poorly documented and require further investigation.

Stable knockdown of ASH1L was achieved in osteosarcoma cell lines to assess its effect on cell migration and invasion. Functional assays revealed that ASH1L silencing significantly suppressed osteosarcoma progression in vitro. EMT is recognized as a crucial biological process facilitating tumor cell invasion and dissemination from primary tumors [112–114]. Concurrently, interference with ASH1L reduced the expression of mesenchymal markers compared to the shNC group, suggesting a potential role in EMT. To further explore the underlying mechanisms, GSEA enrichment analysis was performed on an osteosarcoma meta-cohort. The "MTOR_UP.N4.V1_DN" gene set was enriched in the low-ASH1L expression subgroup, suggesting an association between ASH1L and AKT/mTOR pathway. This pathway is known to induce EMT through mechanisms such as cytoskeletal reorganization, proteasomal degradation of NFAT, and upregulation of EMT transcription factors [115–117]. This study demonstrates that ASH1L overexpression increases p-AKT and p-mTOR levels without affecting total protein concentrations. These results support the hypothesis that ASH1L promotes EMT and metastasis via the AKT/mTOR pathway. Furthermore, Fig. 9 illustrates the development of an ASH1L-derived risk stratification system for osteosarcoma, constructed using ASH1L-related DEGs, LASSO regression, and multivariate Cox analysis. Comparative ROC curve analysis across multiple cohorts demonstrated the superior predictive performance of the ADPI. Finally, a nomogram was established, integrating clinical variables and the ADPI to provide a robust tool for individualized risk assessment in osteosarcoma patients.

In summary, the current study has important implications for characterizing prognostic histone acetylation modulators in osteosarcoma. Further exploration of histone acetylation modification patterns, particularly the biological function of ASH1L, will be important for improving patient risk stratification and guiding personalized therapeutic strategies. However, it is imperative to acknowledge several limitations. Firstly, the relatively limited sample size of osteosarcoma necessitates additional validation of the long-term predictive performance in larger, multicenter cohorts. Secondly, our study only performed in vitro experiments and lacked in vivo animal experiments, which is a research area we will continue to focus on next. Thirdly, while the limma-voom pipeline provides a statistically rigorous approach to differential expression analysis in the absence of raw count data, future studies with access to raw sequencing data could further validate these findings using negative binomial-based approaches. Most notably, the precise immunomodulatory mechanisms of ASH1L within the tumor microenvironment require systematic investigation. Given our findings of distinct immune landscape patterns between C1 and C2 clusters (particularly the association of ASH1L-enriched

C2 with immune suppression), future studies should specifically examine how ASH1L-mediated histone modifications regulate immune cell infiltration and function.

5 Conclusion

Overall, our analysis offers novel insights into the correlation between histone acetylation modification patterns, outcomes, clinical parameters, and immune landscape characterization in osteosarcoma. Furthermore, this study elucidated the role of ASH1L in promoting AKT/mTOR signal transduction and EMT process in osteosarcoma, suggesting that it may serve as a promising therapeutic target.

Supplementary Information

The online version contains supplementary material available at https://doi.org/10.1007/s12672-025-02920-6.

Supplementary Material 1

Supplementary Material 2

Supplementary Material 3

Supplementary Material 4

Acknowledgements
We are very grateful to all the scholars who maintain public databases.

Author contributions
Chenlie Ni: Writing-original draft, Conceptualization, Data curation, Formal analysis, Investigation, Methodology, Software, Validation, Visualization. Qiwen Sun: Data curation, Validation. Haibo Yin: Supervision, Visualization.

Funding
This study was not supported by any funds.

Data availability
The clinical data and sequencing data of osteosarcoma patients, comprising 138 tumor samples, were obtained from GEO database (https://www.ncbi.nlm.nih.gov/geo/) and the TARGET database (https://ocg.cancer.gov/programs/target). All data are available from the corresponding author upon reasonable request.

Declarations

Competing interests
The authors declare no competing interests.

Received: 11 February 2025 / Accepted: 5 June 2025
Published online: 12 June 2025

References

1. Xin ZF, Kim YK, Jung ST. Risedronate inhibits human osteosarcoma cell invasion. J Experimental Clin cancer Research: CR. 2009;28:105.
2. Wang X, Qin G, Liang X, Wang W, Wang Z, Liao D, et al. Targeting the CK1α/CBX4 axis for metastasis in osteosarcoma. Nat Commun. 2020;11:1141.
3. Wang C, Meng Y, Zhao J, Ma J, Zhao Y, Gao R, et al. Deubiquitinase USP13 regulates glycolytic reprogramming and progression in osteosarcoma by stabilizing METTL3/m(6)A/ATG5 axis. Int J Biol Sci. 2023;19:2289–303.
4. Ge J, Yang N, Yang Y, Yu H, Yang X, Wang Y, et al. The combination of eddy thermal effect of biodegradable magnesium with immune checkpoint Blockade shows enhanced efficacy against osteosarcoma. Bioactive Mater. 2023;25:73–85.
5. Lu SL, Wang YH, Liu GF, Wang L, Li Y, Guo ZY, et al. Graphene oxide Nanoparticle-Loaded ginsenoside Rg3 improves photodynamic therapy in inhibiting malignant progression and stemness of osteosarcoma. Front Mol Biosci. 2021;8:663089.
6. Zhang Y, Ru N, Xue Z, Gan W, Pan R, Wu Z, et al. The role of mitochondria-related LncRNAs in characterizing the immune landscape and supervising the prognosis of osteosarcoma. J Bone Oncol. 2023;43:100506.
7. Lin SL, Yang SY, Tsai CH, Fong YC, Chen WL, Liu JF, et al. Nerve growth factor promote VCAM-1-dependent monocyte adhesion and M2 polarization in osteosarcoma microenvironment: implications for larotrectinib therapy. Int J Biol Sci. 2024;20:4114–27.
8. Yang Z, Liu J, Lu Y. Doxorubicin and CD–CUR inclusion complex co–loaded in thermosensitive hydrogel PLGA–PEG–PLGA localized administration for osteosarcoma. Int J Oncol. 2020;57:433–44.
9. Si M, Xia Y, Cong M, Wang D, Hou Y, Ma H. In situ Co-Delivery of doxorubicin and cisplatin by injectable thermosensitive hydrogels for enhanced osteosarcoma treatment. Int J Nanomed. 2022;17:1309–22.

10. Xia H, Hao M, Li K, Chen X, Yu L, Qiu J et al. CD44 and HAP-Conjugated hADSCs as Living Materials for Targeted Tumor Therapy and Bone Regeneration. Adv Sci (Weinheim, Baden-Wurttemberg, Germany). 2023; 10: e2206393.
11. Morrow JJ, Bayles I, Funnell APW, Miller TE, Saiakhova A, Lizardo MM, et al. Positively selected enhancer elements endow osteosarcoma cells with metastatic competence. Nat Med. 2018;24:176–85.
12. Timmerman RD, Bizekis CS, Pass HI, Fong Y, Dupuy DE, Dawson LA, et al. Local surgical, ablative, and radiation treatment of metastases. Cancer J Clin. 2009;59:145–70.
13. Li M, Jin X, Li H, Wu G, Wang S, Yang C, et al. Key genes with prognostic values in suppression of osteosarcoma metastasis using comprehensive analysis. BMC Cancer. 2020;20:65.
14. Bayles I, Krajewska M, Pontius WD, Saiakhova A, Morrow JJ, Bartels C, et al. Ex vivo screen identifies CDK12 as a metastatic vulnerability in osteosarcoma. J Clin Investig. 2019;129:4377–92.
15. Bannister AJ, Kouzarides T. Regulation of chromatin by histone modifications. Cell Res. 2011;21:381–95.
16. Jenuwein T, Allis CD. Translating the histone code. Science (New York, NY). 2001; 293: 1074-80
17. Zhang Y, Sun Z, Jia J, Du T, Zhang N, Tang Y, et al. Overview of Histone Modification. Adv Experimental Med Biology. 2021;1283:1–16.
18. Mariño-Ramírez L, Kann MG, Shoemaker BA, Landsman D. Histone structure and nucleosome stability. Expert Rev Proteomics. 2005;2:719–29.
19. Miziak P, Baran M, Borkiewicz L, Trombik T, Stepulak A. Acetylation of histone H3 in cancer progression and prognosis. Int J Mol Sci. 2024;25(20):10982. https://doi.org/10.3390/ijms252010982
20. Talbert PB, Henikoff S. Histone variants–ancient wrap artists of the epigenome. Nat Rev Mol Cell Biol. 2010;11:264–75.
21. Hu Z, Zhou J, Jiang J, Yuan J, Zhang Y, Wei X, et al. Genomic characterization of genes encoding histone acetylation modulator proteins identifies therapeutic targets for cancer treatment. Nat Commun. 2019;10:733.
22. Grosselin K, Durand A, Marsolier J, Poitou A, Marangoni E, Nemati F, et al. High-throughput single-cell ChIP-seq identifies heterogeneity of chromatin States in breast cancer. Nat Genet. 2019;51:1060–6.
23. Li T, Zhang C, Hassan S, Liu X, Song F, Chen K, et al. Histone deacetylase 6 in cancer. J Hematol Oncol. 2018;11:111.
24. Duan X, Xing Z, Qiao L, Qin S, Zhao X, Gong Y, et al. The role of histone post-translational modifications in cancer and cancer immunity: functions, mechanisms and therapeutic implications. Front Immunol. 2024;15:1495221.
25. Arnaudo AM, Garcia BA. Proteomic characterization of novel histone post-translational modifications. Epigenetics Chromatin. 2013;6:24.
26. Millán-Zambrano G, Burton A, Bannister AJ, Schneider R. Histone post-translational modifications - cause and consequence of genome function. Nat Rev Genet. 2022;23:563–80.
27. Liu R, Wu J, Guo H, Yao W, Li S, Lu Y, et al. Post-translational modifications of histones: mechanisms, biological functions, and therapeutic targets. MedComm. 2023;4:e292.
28. Zhu D, Zhang Y, Wang S. Histone citrullination: a new target for tumors. Mol Cancer. 2021;20:90.
29. Morgan MAJ, Shilatifard A. Epigenetic moonlighting: Catalytic-independent functions of histone modifiers in regulating transcription. Sci Adv. 2023;9:eadg6593.
30. Rothbart SB, Strahl BD. Interpreting the Language of histone and DNA modifications. Biochim Biophys Acta. 2014;1839:627–43.
31. Allfrey VG, Faulkner R, Mirsky AE, Acetylation and methylation of histones and their possible role in, the regulation of RNA synthesis. Proc Natl Acad Sci USA. 1964;51:786–94.
32. Charidemou E, Kirmizis A. A two-way relationship between histone acetylation and metabolism. Trends Biochem Sci. 2024;49:1046–62.
33. Berger SL. The complex Language of chromatin regulation during transcription. Nature. 2007;447:407–12.
34. Imhof A, Yang XJ, Ogryzko VV, Nakatani Y, Wolffe AP, Ge H. Acetylation of general transcription factors by histone acetyltransferases. Curr Biology: CB. 1997;7:689–92.
35. Marmorstein R, Zhou MM. Writers and readers of histone acetylation: structure, mechanism, and Inhibition. Cold Spring Harb Perspect Biol. 2014;6:a018762.
36. MacDonald VE, Howe LJ. Histone acetylation: where to go and how to get there. Epigenetics. 2009;4:139–43.
37. Ghobrial IM, Campigotto F, Murphy TJ, Boswell EN, Banwait R, Azab F, et al. Results of a phase 2 trial of the single-agent histone deacetylase inhibitor Panobinostat in patients with relapsed/refractory Waldenström macroglobulinemia. Blood. 2013;121:1296–303.
38. Xiao Y, Zhang Y, Hu Y, Zhang X, Tan J, Yao S, et al. Advances in the study of posttranslational modifications of histones in head and neck squamous cell carcinoma. Clin Epigenetics. 2024;16:165.
39. McGuire JJ, Nerlakanti N, Lo CH, Tauro M, Utset-Ward TJ, Reed DR, et al. Histone deacetylase Inhibition prevents the growth of primary and metastatic osteosarcoma. Int J Cancer. 2020;147:2811–23.
40. Nerlakanti N, McGuire JJ, Bishop RT, Nasr MM, Li T, Reed DR, et al. Histone deacetylase upregulation of neuropilin-1 in osteosarcoma is essential for pulmonary metastasis. Cancer Lett. 2024;606:217302.
41. Huang JH, Xu Y, Lin FY. The Inhibition of microRNA-326 by SP1/HDAC1 contributes to proliferation and metastasis of osteosarcoma through promoting SMO expression. J Cell Mol Med. 2020;24:10876–88.
42. Song W, Tai YT, Tian Z, Hideshima T, Chauhan D, Nanjappa P, et al. HDAC Inhibition by LBH589 affects the phenotype and function of human myeloid dendritic cells. Leukemia. 2011;25:161–8.
43. Yuan Q, Wu Y, Xue C, Zhao D, Wang H, Shen Y. KAT7 serves as an oncogenic gene and regulates CCL3 expression via STAT1 signaling in osteosarcoma. Biochem Biophys Res Commun. 2024;722:150156.
44. Gao YY, Ling ZY, Zhu YR, Shi C, Wang Y, Zhang XY, et al. The histone acetyltransferase HBO1 functions as a novel oncogenic gene in osteosarcoma. Theranostics. 2021;11:4599–615.
45. Chandrashekar DS, Afaq F, Karthikeyan SK, Athar M, Shrestha S, Singh R, et al. Bromodomain inhibitor treatment leads to overexpression of multiple kinases in cancer cells. Volume 57. New York, NY: Neoplasia; 2024. p. 101046.
46. Jiang Y, Wang G, Mu H, Ma X, Wang Z, Lv Y, et al. Bromodomain Inhibition attenuates the progression and sensitizes the chemosensitivity of osteosarcoma by repressing GP130/STAT3 signaling. Front Oncol. 2021;11:642134.
47. Luo SH, Tian JM, Chu Y, Zhu HY, Ni JD, Huang J. The BRD4-SRPK2-SRSF2 signal modulates the splicing efficiency of ACSL3 pre-mRNA and influences erastin-induced ferroptosis in osteosarcoma cells. Cell Death Dis. 2023;14:760.
48. Long M, Hou W, Liu Y, Hu T. A histone acetylation modulator gene signature for classification and prognosis of breast Cancer. Curr Oncol (Toronto Ont). 2021;28:928–39.

49. Jiang Y, Guo X, Liu L, Rode S, Wang R, Liu H, et al. Metagenomic characterization of lysine acetyltransferases in human cancer and their association with clinicopathologic features. Cancer Sci. 2020;111:1829–39.
50. Bacci G, Rocca M, Salone M, Balladelli A, Ferrari S, Palmerini E, et al. High grade osteosarcoma of the extremities with lung metastases at presentation: treatment with neoadjuvant chemotherapy and simultaneous resection of primary and metastatic lesions. J Surg Oncol. 2008;98:415–20.
51. Zhang F, Yan T, Guo W, Sun K, Wang S, Bao X, et al. Novel oncogene COPS3 interacts with Beclin1 and Raf-1 to regulate metastasis of osteosarcoma through autophagy. J Experimental Clin cancer Research: CR. 2018;37:135.
52. Yu B, Geng C, Wu Z, Zhang Z, Zhang A, Yang Z, et al. A CIC-related-epigenetic factors-based model associated with prediction, the tumor microenvironment and drug sensitivity in osteosarcoma. Sci Rep. 2024;14:1308.
53. Zhu J, Yuan J, Arya S, Du Z, Liu X, Jia J. Exploring the immune microenvironment of osteosarcoma through T cell exhaustion-associated gene expression: a study on prognosis prediction. Front Immunol. 2023;14:1265098.
54. Li Z, Xue Y, Huang X, Xiao G. Stratifying osteosarcoma patients using an epigenetic modification-related prognostic signature: implications for immunotherapy and chemotherapy selection. Translational cancer Res. 2024;13:3556–74.
55. Hong W, Yuan H, Gu Y, Liu M, Ji Y, Huang Z, et al. Immune-related prognosis biomarkers associated with osteosarcoma microenvironment. Cancer Cell Int. 2020;20:83.
56. Bakir B, Chiarella AM, Pitarresi JR, Rustgi AK. EMT, MET, plasticity, and tumor metastasis. Trends Cell Biol. 2020;30:764–76.
57. Pastushenko I, Blanpain C. EMT transition States during tumor progression and metastasis. Trends Cell Biol. 2019;29:212–26.
58. Peng Y, Wang Y, Zhou C, Mei W, Zeng C. PI3K/Akt/mTOR pathway and its role in Cancer therapeutics: are we making headway?? Front Oncol. 2022;12:819128.
59. Deng J, Bai X, Feng X, Ni J, Beretov J, Graham P, et al. Inhibition of PI3K/Akt/mTOR signaling pathway alleviates ovarian cancer chemoresistance through reversing epithelial-mesenchymal transition and decreasing cancer stem cell marker expression. BMC Cancer. 2019;19:618.
60. Karimi Roshan M, Soltani A, Soleimani A, Rezaie Kahkhaie K, Afshari AR, Soukhtanloo M. Role of AKT and mTOR signaling pathways in the induction of epithelial-mesenchymal transition (EMT) process. Biochimie. 2019;165:229–34.
61. Hwang YR, Lee KM, Kim HG, Na K. Diagnostic challenge in rapidly growing Langerhans cell histiocytosis with aneurysmal bone cyst in the maxilla: A case report. Diagnostics (Basel). 2022;12(2):400. https://doi.org/10.3390/diagnostics12020400
62. Bertin H, Guilho R, Brion R, Amiaud J, Battaglia S, Moreau A, et al. Jaw osteosarcoma models in mice: first description. J Translational Med. 2019;17:56.
63. Zhang Y, Pan R, Li K, Cheang LH, Zhao J, Zhong Z, et al. HSPD1 supports osteosarcoma progression through stabilizing ATP5A1 and thus activation of akt/mtor signaling. Int J Biol Sci. 2024;20:5162–90.
64. Wang S, Zhong L, Li Y, Xiao D, Zhang R, Liao D, et al. Up-regulation of PCOLCE by TWIST1 promotes metastasis in osteosarcoma. Theranostics. 2019;9:4342–53.
65. Zhang J, Wang S, Bai Y, Ali AM, Deng J, Chen Y et al. miR-197-3p promotes osteosarcoma stemness and chemoresistance by inhibiting SPOPL. J Clin Med. 2023;12(3):1177. https://doi.org/10.3390/jcm12031177
66. Li Y, Seto E. HDACs and HDAC Inhibitors in Cancer Development and Therapy. Cold Spring Harbor perspectives in medicine. 2016; 6.
67. Ramaiah MJ, Tangutur AD, Manyam RR. Epigenetic modulation and Understanding of HDAC inhibitors in cancer therapy. Life Sci. 2021;277:119504.
68. Bajbouj K, Al-Ali A, Ramakrishnan RK, Saber-Ayad M, Hamid Q. Histone modification in NSCLC: molecular mechanisms and therapeutic targets. Int J Mol Sci. 2021;22(21):11701. https://doi.org/10.3390/ijms222111701
69. Dang F, Wei W. Targeting the acetylation signaling pathway in cancer therapy. Sem Cancer Biol. 2022;85:209–18.
70. Huang B, Wang J, Sun M, Chen X, Xu D, Li ZP, et al. Feasibility of multi-parametric magnetic resonance imaging combined with machine learning in the assessment of necrosis of osteosarcoma after neoadjuvant chemotherapy: a preliminary study. BMC Cancer. 2020;20:322.
71. Chen Y, Cao J, Zhang N, Yang B, He Q, Shao X, et al. Advances in differentiation therapy for osteosarcoma. Drug Discovery Today. 2020;25:497–504.
72. Xiong Y, Wang Z, Zhou Q, Zeng H, Zhang H, Liu Z et al. Identification and validation of dichotomous immune subtypes based on intratumoral immune cells infiltration in clear cell renal cell carcinoma patients. J Immunother Cancer. 2020;8(1):e000447. https://doi.org/10.1136/jitc-2019-000447
73. Quail DF, Joyce JA. Microenvironmental regulation of tumor progression and metastasis. Nat Med. 2013;19:1423–37.
74. Bulla R, Tripodo C, Rami D, Ling GS, Agostinis C, Guarnotta C, et al. C1q acts in the tumour microenvironment as a cancer-promoting factor independently of complement activation. Nat Commun. 2016;7:10346.
75. Gajewski TF, Schreiber H, Fu YX. Innate and adaptive immune cells in the tumor microenvironment. Nat Immunol. 2013;14:1014–22.
76. Nguyen TT, Lee HS, Burt BM, Wu J, Zhang J, Amos CI, et al. A lepidic gene signature predicts patient prognosis and sensitivity to immunotherapy in lung adenocarcinoma. Genome Med. 2022;14:5.
77. Hu Y, Li Z, Zhang Y, Wu Y, Liu Z, Zeng J, et al. The evolution of tumor microenvironment in gliomas and its implication for target therapy. Int J Biol Sci. 2023;19:4311–26.
78. Zhao X, Ren T, Li S, Wang X, Hou R, Guan Z, et al. A new perspective on the therapeutic potential of tumor metastasis: targeting the metabolic interactions between TAMs and tumor cells. Int J Biol Sci. 2024;20:5109–26.
79. Mao X, Xu J, Wang W, Liang C, Hua J, Liu J, et al. Crosstalk between cancer-associated fibroblasts and immune cells in the tumor microenvironment: new findings and future perspectives. Mol Cancer. 2021;20:131.
80. Czajka-Francuz P, Prendes MJ, Mankan A, Quintana Á, Pabla S, Ramkissoon S, et al. Mechanisms of immune modulation in the tumor microenvironment and implications for targeted therapy. Front Oncol. 2023;13:1200646.
81. Yan H, Ju X, Huang A, Yuan J. Advancements in technology for characterizing the tumor immune microenvironment. Int J Biol Sci. 2024;20:2151–67.
82. Zhu T, Han J, Yang L, Cai Z, Sun W, Hua Y, et al. Immune microenvironment in osteosarcoma: components, therapeutic strategies and clinical applications. Front Immunol. 2022;13:907550.
83. Cai S, Chen Z, Wang Y, Wang M, Wu J, Tong Y, et al. Reducing PD-L1 expression with a self-assembled nanodrug: an alternative to PD-L1 antibody for enhanced chemo-immunotherapy. Theranostics. 2021;11:1970–81.
84. St Paul M, Ohashi PS. The roles of CD8(+) T cell subsets in antitumor immunity. Trends Cell Biol. 2020;30:695–704.

85. Bald T, Krummel MF, Smyth MJ, Barry KC. The NK cell-cancer cycle: advances and new challenges in NK cell-based immunotherapies. Nat Immunol. 2020;21:835–47.
86. Lei X, Lei Y, Li JK, Du WX, Li RG, Yang J, et al. Immune cells within the tumor microenvironment: biological functions and roles in cancer immunotherapy. Cancer Lett. 2020;470:126–33.
87. Yu S, Xiong G, Zhao S, Tang Y, Tang H, Wang K, et al. Nanobodies targeting immune checkpoint molecules for tumor immunotherapy and immunoimaging (Review). Int J Mol Med. 2021;47:444–54.
88. de Miguel M, Calvo E. Clinical challenges of immune checkpoint inhibitors. Cancer Cell. 2020;38:326–33.
89. Hargadon KM, Johnson CE, Williams CJ. Immune checkpoint Blockade therapy for cancer: an overview of FDA-approved immune checkpoint inhibitors. Int Immunopharmacol. 2018;62:29–39.
90. Chen X, Lu Q, Zhou H, Liu J, Nadorp B, Lasry A, et al. A membrane-associated MHC-I inhibitory axis for cancer immune evasion. Cell. 2023;186:3903–e2021.
91. Jiang N, Yu Y, Wu D, Wang S, Fang Y, Miao H, et al. HLA and tumour immunology: immune escape, immunotherapy and immune-related adverse events. J Cancer Res Clin Oncol. 2023;149:737–47.
92. Nakamura T, Blechman J, Tada S, Rozovskaia T, Itoyama T, Bullrich F, et al. huASH1 protein, a putative transcription factor encoded by a human homologue of the Drosophila ash1 gene, localizes to both nuclei and cell-cell tight junctions. Proc Natl Acad Sci USA. 2000;97:7284–9.
93. Zhang C, Xu L, Zheng X, Liu S, Che F. Role of Ash1l in tourette syndrome and other neurodevelopmental disorders. Dev Neurobiol. 2021;81:79–91.
94. Tripoulas N, LaJeunesse D, Gildea J, Shearn A. The Drosophila ash1 gene product, which is localized at specific sites on polytene chromosomes, contains a SET domain and a PHD finger. Genetics. 1996;143:913–28.
95. Gregory GD, Vakoc CR, Rozovskaia T, Zheng X, Patel S, Nakamura T, et al. Mammalian ASH1L is a histone methyltransferase that occupies the transcribed region of active genes. Mol Cell Biol. 2007;27:8466–79.
96. Xie M, Zhang L, Han L, Huang L, Huang Y, Yang M, et al. The ASH1L-AS1-ASH1L axis controls NME1-mediated activation of the RAS signaling in gastric cancer. Oncogene. 2023;42:3435–45.
97. Yu XH, Xie Y, Yu J, Zhang KN, Guo ZB, Wang D, et al. Loss-of-function mutations of microRNA-142-3p promote ASH1L expression to induce immune evasion and hepatocellular carcinoma progression. World J Gastroenterol. 2025;31:101198.
98. Xia M, Liu J, Liu S, Chen K, Lin H, Jiang M, et al. Ash1l and lnc-Smad3 coordinate Smad3 locus accessibility to modulate iTreg polarization and T cell autoimmunity. Nat Commun. 2017;8:15818.
99. Xia M, Liu J, Wu X, Liu S, Li G, Han C, et al. Histone methyltransferase Ash1l suppresses interleukin-6 production and inflammatory autoimmune diseases by inducing the ubiquitin-editing enzyme A20. Immunity. 2013;39:470–81.
100. Zhao L, Liu Y, Ma B, Liu X, Wei R, Nian H. METTL3 inhibits autoreactive Th17 cell responses in experimental autoimmune uveitis via stabilizing ASH1L mRNA. FASEB J. 2023; 37: e22803.
101. Liu N, He J, Fan D, Gu Y, Wang J, Li H, et al. Circular RNA circTmem241 drives group III innate lymphoid cell differentiation via initiation of Elk3 transcription. Nat Commun. 2022;13:4711.
102. Du Y, Wu S, Xi S, Xu W, Sun L, Yan J et al. ASH1L in hepatoma cells and hepatic stellate cells promotes fibrosis-associated hepatocellular carcinoma by modulating tumor-associated macrophages. Adv Sci (Weinheim, Baden-Wurttemberg, Germany). 2024; 11: e2404756.
103. Yu M, Jia Y, Ma Z, Ji D, Wang C, Liang Y, et al. Structural insight into ASH1L PHD finger recognizing methylated histone H3K4 and promoting cell growth in prostate cancer. Front Oncol. 2022;12:906807.
104. Rogawski DS, Deng J, Li H, Miao H, Borkin D, Purohit T, et al. Discovery of first-in-class inhibitors of ASH1L histone methyltransferase with anti-leukemic activity. Nat Commun. 2021;12:2792.
105. Xu B, Qin T, Yu J, Giordano TJ, Sartor MA, Koenig RJ. Novel role of ASH1L histone methyltransferase in anaplastic thyroid carcinoma. J Biol Chem. 2020;295:8834–45.
106. Rogawski DS, Ndoj J, Cho HJ, Maillard I, Grembecka J, Cierpicki T. Two loops undergoing concerted dynamics regulate the activity of the ASH1L histone methyltransferase. Biochemistry. 2015;54:5401–13.
107. Ding B, Yan L, Zhang Y, Wang Z, Zhang Y, Xia D, et al. Analysis of the role of mutations in the KMT2D histone lysine methyltransferase in bladder cancer. FEBS Open Bio. 2019;9:693–706.
108. Demelash A, Rudrabhatla P, Pant HC, Wang X, Amin ND, McWhite CD, et al. Achaete-scute homologue-1 (ASH1) stimulates migration of lung cancer cells through Cdk5/p35 pathway. Mol Biol Cell. 2012;23:2856–66.
109. Colamaio M, Puca F, Ragozzino E, Gemei M, Decaussin-Petrucci M, Aiello C, et al. miR-142-3p down-regulation contributes to thyroid follicular tumorigenesis by targeting ASH1L and MLL1. J Clin Endocrinol Metab. 2015;100:E59–69.
110. Trissal MC, Wong TN, Yao JC, Ramaswamy R, Kuo I, Baty J, et al. MIR142 Loss-of-Function mutations derepress ASH1L to increase HOXA gene expression and promote leukemogenesis. Cancer Res. 2018;78:3510–21.
111. Zhu L, Li Q, Wong SH, Huang M, Klein BJ, Shen J, et al. ASH1L links histone H3 lysine 36 dimethylation to MLL leukemia. Cancer Discov. 2016;6:770–83.
112. Gundamaraju R, Lu W, Paul MK, Jha NK, Gupta PK, Ojha S, et al. Autophagy and EMT in cancer and metastasis: who controls whom? Biochim Et Biophys Acta Mol Basis Disease. 2022;1868:166431.
113. Banyard J, Bielenberg DR. The role of EMT and MET in cancer dissemination. Connect Tissue Res. 2015;56:403–13.
114. Katsuno Y, Lamouille S, Derynck R. TGF-β signaling and epithelial-mesenchymal transition in cancer progression. Curr Opin Oncol. 2013;25:76–84.
115. Sheng S, Qiao M, Pardee AB. Metastasis and AKT activation. J Cell Physiol. 2009;218:451–4.
116. Tian W, Li J, Wang Z, Zhang T, Han Y, Liu Y, et al. HYD-PEP06 suppresses hepatocellular carcinoma metastasis, epithelial-mesenchymal transition and cancer stem cell-like properties by inhibiting PI3K/AKT and WNT/β-catenin signaling activation. Acta Pharm Sinica B. 2021;11:1592–606.
117. Qiao M, Sheng S, Pardee AB. Metastasis and AKT activation. Cell Cycle (Georgetown Tex). 2008;7:2991–6.

Publisher's note